Fast scanning heterodyne receiver for the measurement of the time evolution of the electron temperature profile on the Tokamak Fusion Test Reactor

G. Taylor, P. Efthimion, M. McCarthy, V. Arunasalam, R. Bitzer,[a] J. Bryer, R. Cutler, E. Fredd, M. A. Goldman, and D. Kaufman

Plasma Physics Laboratory, Princeton University, Princeton, New Jersey 08544

(Received 18 May 1984; accepted for publication 11 July 1984)

Two fast scanning heterodyne receivers, swept between 75–110 and 110–170 GHz in 2 ms every 4 ms, were developed to measure the electron cyclotron emission on the horizontal midplane of the Tokamak Fusion Test Reactor (TFTR) plasma. An absolute, *in situ* calibration technique enables the determination of the profile of the plasma electron temperature from the cyclotron emission intensity. The 4-ms repetition rate of the receiver allowed the resolution of "sawtooth" fluctuations of temperature, whose period was 10–100 ms, in profiles with central temperatures of 1–2.5 keV.

INTRODUCTION

In dense, high-temperature plasma the intensity of electron cyclotron emission for the fundamental and second harmonic has been observed to be at the blackbody level, so that the emission intensity is proportional to the local electron temperature.[1–6] In tokamaks the toroidal magnetic field is inversely proportional to the major radius, and the cyclotron frequency, therefore, corresponds to a unique radial position. The incident microwave power P at a receiver antenna is proportional to the cyclotron emission intensity

$$P(R) \propto kT_e(R)\Delta F(1 - e^{-\tau}),$$

where T_e is the electron temperature, k is Boltzmann's constant, ΔF is the receiver bandwidth, and τ is the optical depth of the emitting layer. The optical depth is dependent on the plasma geometry, electron temperature, and density (n_e).[6] For example, for the plasma measurements reported here the ordinary mode emission at the fundamental cyclotron frequency was used, so that for a $T_e \approx 1\text{keV}, n_e \approx 2\times 10^{13}$ cm^{-3} plasma at a toroidal field of 30 kG, $\tau \approx 8$. When $\tau \gtrsim 2$, the emission is essentially blackbody. Under these conditions the power received by the radiometer is proportional to the electron temperature. In addition, the reflectivity of the tokamak vacuum vessel can considerably enhance the emission when $\tau \lesssim 2$ so the emission intensity can be at the blackbody level.

The study of the evolution of the electron temperature versus plasma major radius $T_e(R)$ is essential to the understanding of transport processes in tokamaks. Other electron temperature profile diagnostics, for example, TV laser Thomson scattering[7] provide only one or two temperature profiles during a plasma discharge with a duration of several seconds. The scanning cyclotron radiometer provides many $T_e(R)$ profiles during a discharge.

For the Tokamak Fusion Test Reactor (TFTR) the electron cyclotron radiometer is required to measure radial temperature profiles with edge temperatures as low as 50 eV and central temperatures up to 20 keV. In addition, the toroidal magnetic field, which ranges from 10–50 kG, and the large plasma diameter necessitate a wide radiometric frequency coverage. To achieve full radiometric capability in TFTR, a frequency coverage of 75–220 GHz is necessary. At present, receivers are operating in the bands 75–110 and 110–170 GHz, while TFTR operates with a toroidal field of up to 30 kG.

I. RADIOMETER DESIGN

Figure 1 shows an overall schematic of the TFTR cyclotron radiometer. A periscope attached to the TFTR vacuum vessel was designed so that there is no direct path to the vacuum windows for impurities from the discharge. The periscope contains a rotatable, chromium plated, aluminum

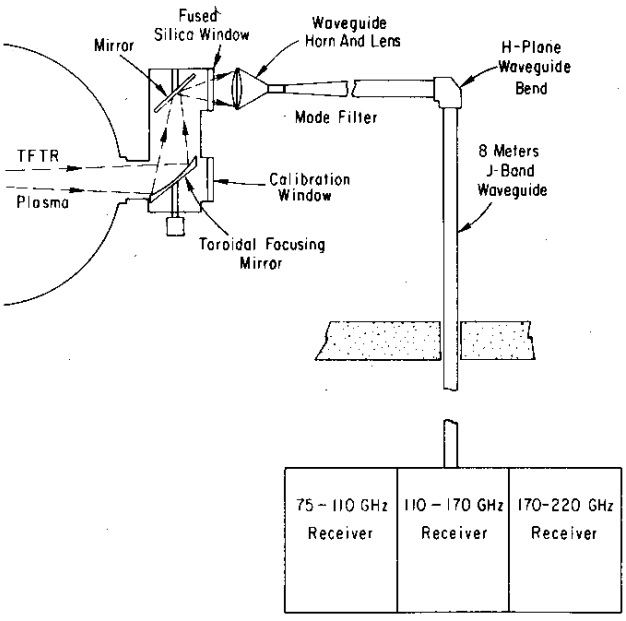

FIG. 1. Schematic layout of TFTR radiometer.

 0034-6748/84/111739-05$01.30

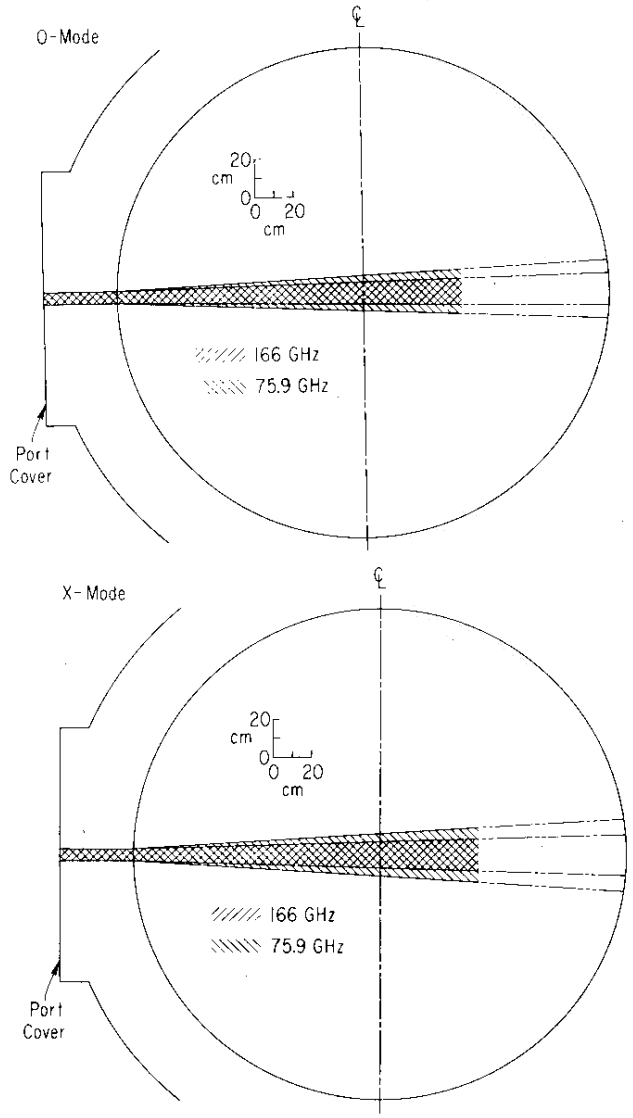

FIG. 2. Field of view of radiometer showing a schematic of the TFTR plasma for (a) O-mode and (b) X-mode cyclotron emission. The large circle indicates the edge of an 83-cm minor radius plasma.

alloy toroidal mirror and a fixed, plane aluminum alloy mirror, which directs cyclotron radiation from the plasma through a 15-cm-diam fused silica vacuum window. A toroidal focusing mirror was selected to optimize the imaging of the cyclotron emission while minimizing the cost of fabrication. Chromium plating was employed to suppress arc damage to the aluminum alloy mirror surface during glow discharge cleaning. Figure 2 shows the measured viewing pattern for the periscope optics for both ordinary and extraordinary mode radiation at 75.9 and 166 GHz. Diffraction is significant at the lower frequency, and in the presence of plasma and additional refractive effect spreads the beam. However, for electron densities under normal operating conditions, typically $\lesssim 10^{20}\ m^{-3}$, plasma refraction is minimal. The windows have a 2° wedge to prevent interference from multiple internal reflections. A Rexalyte lens and a conical horn direct the radiation to taper into a TE_{11}^{*}–TE_{10} transition in WR-10 guide. To prevent higher-order modes, a section of reduced height guide is included in the antenna feed.

An 8-m, overmoded, J-band waveguide (WR-137) carries the radiation to three receivers covering 75–220 GHz. A straight section of WR-10 fundamental guide behind the horn can be replaced with a 90° twisted guide to observe extraordinary mode emission. The insertion loss of the WR-10 to WR-137 taper is approximately 0.3 dB. The 8-m, J-band waveguide run has a relatively low loss of 0.26 dB/m.

Two receivers are operational at present, these cover the 75–110- and 110–170-GHz bands. To distribute incident power to the receivers, a four-port power splitting network, which has a smooth frequency response without signifcant moding or resonances, has been designed.[8] This network has good isolation between receivers so that local oscillator leakage power and reflected incident power do not couple from one receiver to another. The splitting network introduces a loss of about 5 dB between the input port and the 75–110-GHz receiver and 4 dB between the input port and the 110–170-GHz receiver. Gaussian tapers with a 0.3-dB loss provide transition between the WR-137 guide for the splitter network ports and the WR-10 and WR-7 single-mode guides

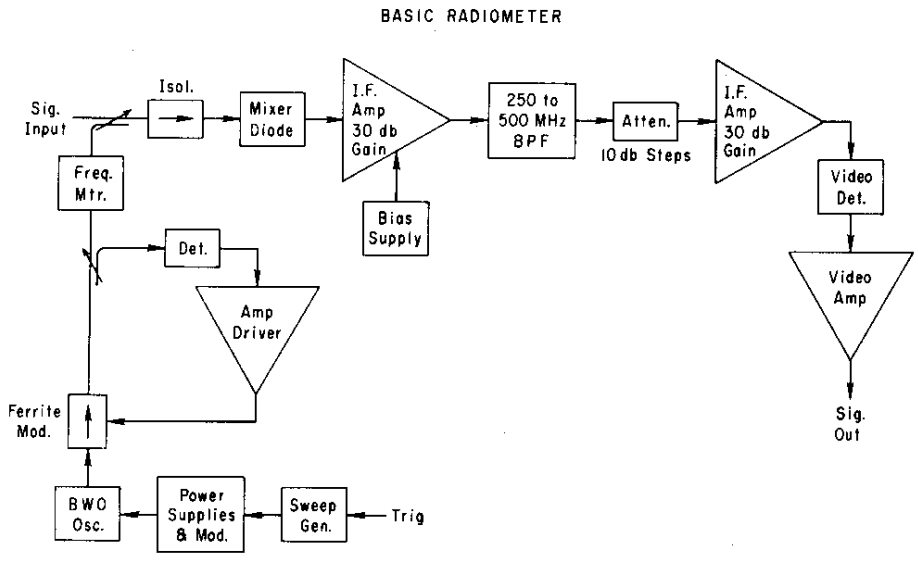

FIG. 3. Schematic of 75–110-GHz receiver.

for the 75–110-and110–170-GHz receivers, respectively.

A schematic of the 75–110-GHz receiver is shown in Fig. 3. The design is a development of the radiometer described by Efthimion *et al.*[9] The signal from the plasma is mixed with radiation from a Siemens RW0–110N backward wave oscillator (BWO) in a broadband, single-ended mixer. The BWO power is leveled with a ferrite modulator in a feedback loop and electronically swept in 4 ms (including a 2-ms flyback) over the frequency range 75–110 GHz by a 2-kV voltage ramp produced by a high-voltage amplifier connected to an electronics control chassis. In addition to generating a ramp voltage, the electronics package can provide 256 programmable voltage levels. The electronics can be programmed to provide one of three modes: a ramp mode providing ramps every 4 ms, a dwell mode where the BWO is set to one frequency continuously, and a ramp–dwell mode where the BWO is alternately ramped and then made to dwell for up to 100 ms, at one frequency.

The microwave mixer output is passed through two stages of IF amplification each with 30 dB of gain and a pass band of 250–500 MHz to provide rejection of BWO noise below 250 MHz. A step attenuator provides gain adjustment in 10-dB steps, and a 250–500-MHz filter between the two amplifier stages gives additional BWO noise rejection. The output of the final IF amplifier is detected by a Schottky barrier video detector and passed through a 10-kHz bandwidth, output amplifier whose gain is 250.

The 110–170-GHz band receiver is similar to the 75–110-GHz band except that it uses a Siemens RW0–170N and the IF bandwidth is 1–2 GHz in order to reject more strongly the BWO induced noise in the mixer.

Ramp data are sampled at 24 preset voltages during the 2-ms sweep by voltage comparators which are preset to generate a trigger at a specified BWO cathode voltage. In this way samples are taken at fixed values of BWO frequency, guaranteeing frequency synchronous acquisition. Output from each receiver is stored in a 32-kword memory by a transient digitizer. A verification cycle occurs immediately before the plasma discharge which provides a video base line, mixer bias current, and BWO cathode voltage in both ramp and dwell modes. The verification data are digitized and mutiplexed before the plasma data are stored for each discharge. Dwell data are digitized at a 25-kHz rate.

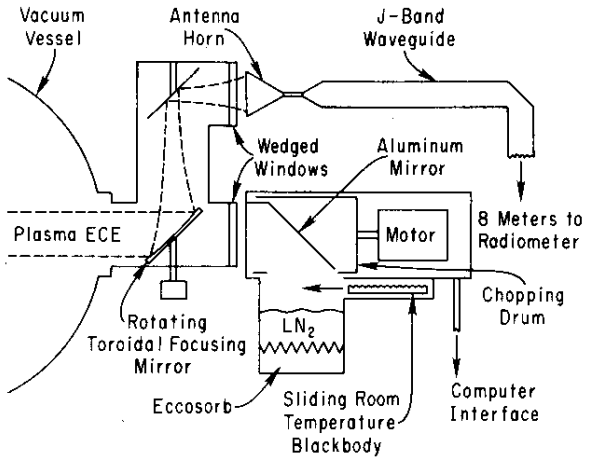

FIG. 4. Schematic diagram of *in situ* calibration system. For calibration measurements the toroidal focusing mirror is rotated to face the cold Eccosorb source.

II. RADIOMETER SPATIAL RESOLUTION

As shown in Fig. 2, the resolution transverse to the major radial direction at the TFTR vacuum vessel center is better than 15 cm at 166 GHz and approximately 20 cm at 75.9 GHz. The resolution in the major radial direction is determined by the bandwidth of the receivers. For the 75–110-GHz band typical resolution is $\approx$2.5 cm and for the 110–170-GHz band $\simeq$5 cm.

III. RADIOMETER CALIBRATION

Absolute, *in situ* calibration of the radiometer employing Dicke[10] switching allowed determination of the plasma electron temperature independent of other plasma diagnostics.

Eccosorb CV immersed in liquid nitrogen was used as a blackbody calibration source. The calibration source was installed on TFTR only during calibration measurements, which were made once a month. A schematic of the calibration system is shown in Fig. 4. The toroidal focusing mirror in the periscope can be rotated away from the TFTR plasma to view the calibration source through a wedged fused silica vacuum window. An Eccosorb covered chopping drum rotates at approximately 3000 rpm so that the radiometer alternately views the cold load and a room-temperature load about 100 times per second. A sliding Eccosorb shutter can be moved to block the view of the cold load.

The calibration source is viewed by the radiometer with the receiver set to dwell at one of the 24 frequencies sampled in the ramp mode. The sensitivity at each frequency is determined directly by synchronously detecting the receiver output with a lock-in amplifier referenced to the chopping frequency of the drum.

Prior to installation on TFTR the 75–110-GHz receiver sensitivity was measured in the laboratory with a lock-in amplifier integration time of 1 s using the Eccosorb cold load, and a sensitivity of 0.1–0.27 μV/K was measured as shown in Fig. 5. The measured noise figure in the laboratory was typically 23 dB or a noise equivalent power $\approx 8\times 10^{-19}$

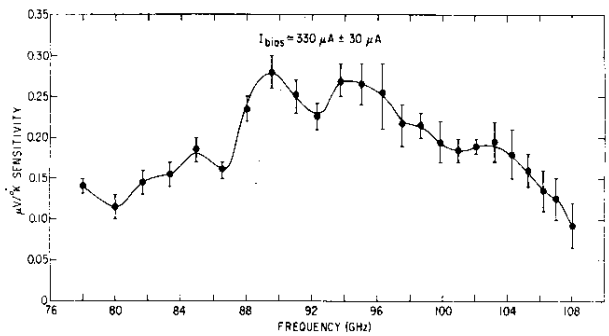

FIG. 5. 75–110-GHz receiver sensitivity vs frequency measured in the laboratory.

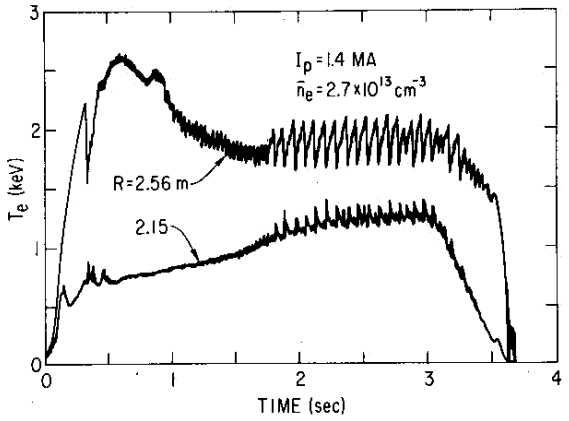

FIG. 6. Electron temperature time history for a 1.4-MA TFTR discharge at two major radii showing large "sawtooth" temperature fluctuations.

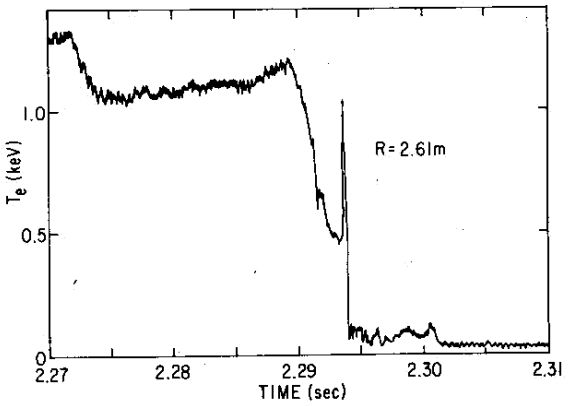

FIG. 8. An example of dwell mode used to capture the electron temperature collapse during a plasma disruption, terminating the discharge.

WHz^{-1}. Comparing the sensitivity curve in Fig. 5 with the sensitivity obtained *in situ* on TFTR, where integration times were 8–25 s, we determined the waveguide loss to be 6–7 dB. The fused quartz windows contributed 0.7 dB to the loss in the 75–110-GHz band and the window through which the calibration source is viewed must be calibrated before installation on the periscope. The calibration technique described here provided calibration accuracies of about 5%–10% for each sample. Calibrated sensitivities for each of the 24 sample frequencies taken during a BWO ramp plus the frequencies of each sample were stored in a calibration data file on the data-acquisition computer.

IV. DATA ANALYSIS AND OPERATION

A data analysis program was written to allow display of electron temperature versus major radius and time. The program utilized the sensitivity factors in the calibration data file created during the calibration and the toroidal field coil current measurements to calculate the major radial position of the data sampled by the radiometer. An example of electron temperature time history data generated by this program is shown in Fig. 6. The electron temperature at two major radial positions is shown during a 1.4-MA plasma current discharge with a minor radius of 0.83 m and a nominal major radius (R) of 2.55 m. The temperature at $R = 2.56$ m, close to the plasma magnetic axis shows large, 80-ms period sawteeth. At $R = 2.15$ m the time history shows inverted sawteeth. These time histories were reconstructed from ramp data. The temperature sawteeth are believed to be important to the transport of energy in the hot plasma core. Electron temperature profile data from this instrument were used extensively in the study of energy confinement in TFTR.[11–13] Figure 7 shows four profiles during the evolution of the electron temperature when the plasma column was compressed by being moved inward in major radius. The curve is a fourth-order polynomial fit to the data. The compression begins at 2 s and is complete after about 20 ms.

Figure 8 shows the application of the programmable dwell mode, where a plasma disruption causes a rapid collapse in central electron temperature from 1 keV in less than 4 ms compared to a plasma current decay time of 10 ms. Figure 9 shows an example of a three-dimensional major radius–time plot of the evolution of temperature sawteeth in a 1.4-MA discharge constructed from a series of ramps. The

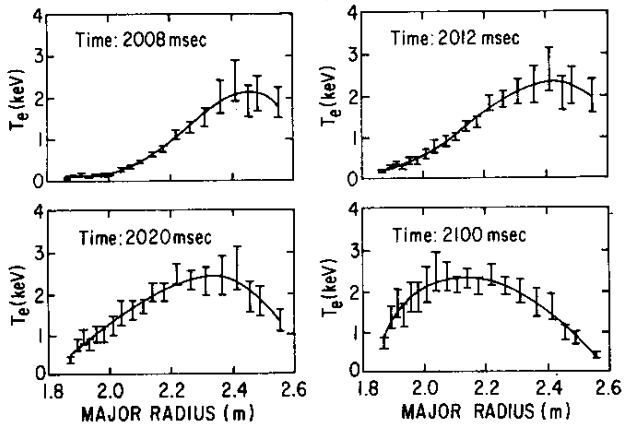

FIG. 7. Profile of electron temperature on TFTR at four times during an adiabatic compression experiment, where the plasma is moved inward in major radius.

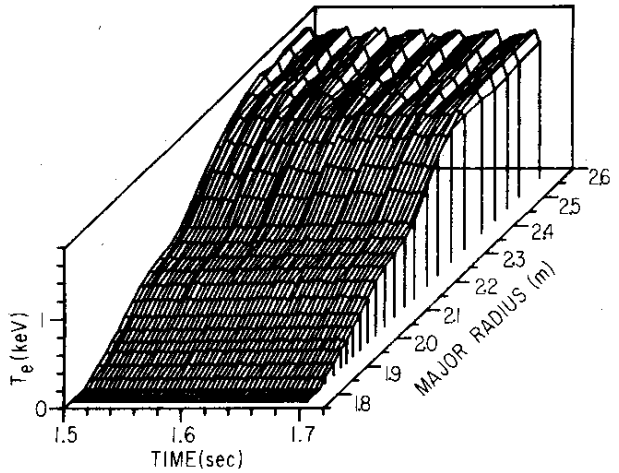

FIG. 9. Three-dimensional major radius–time plot showing electron temperature profile evolution in a 1.4-MA discharge on TFTR.

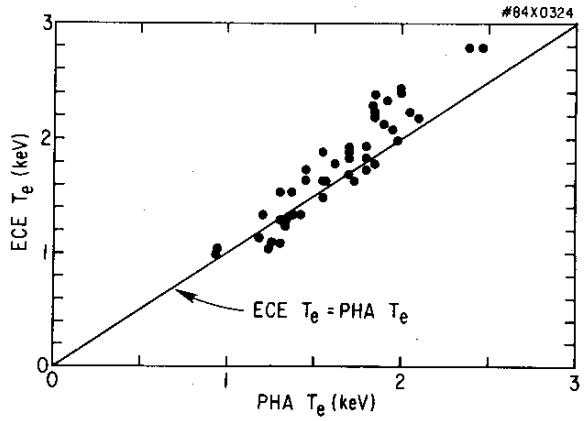

FIG. 10. Comparison between electron cyclotron emission (ECE) and x-ray pulse -height analyzer (PHA) electron temperature data.

spatial and temporal resolution is sufficient to resolve temperature sawteeth.

Figure 10 indicates the degree of agreement between the electron temperature measured by the cyclotron radiometer and the electron temperature derived from x-ray bremsstrahlung by a pulse-height analyzer (PHA).[13,14] In general, agreement was good, within better than 20% between the two diagnostics over a wide range of plasma conditions.

In the future, a third 170–220-GHz receiver will allow the study of plasma discharges with toroidal fields $\gtrsim 40$ kG. A hot load and calibration in ramp mode are being considered which will permit temperature measurement to an accuracy better than 5%.

ACKNOWLEDGMENT

The technical support of M. E. Oldaker and W. M. McCredie is gratefully acknowledged. We would also like to thank K. M. Young, L. C. Johnson, and the many other people on the TFTR staff who helped support and encourage this work. This work was supported under U. S. DOE Contract No. DE-AC02-76-CHO-3073.

[a] RCA Corporation, Astro Electronics Division, Hightstown, NJ.

[1] V. Arunasalam, E. B. Meservey, M. M. Gurnee, and R. C. Davidson, Phys. Fluids **11**, 1076 (1968).
[2] A. E. Costley, R. J. Hastie, J. W. M. Paul, and J. Chamberlain, Phys. Rev. Lett. **33**, 758 (1974).
[3] V. Arunasalam, R. Cano, and J. C. Hosea, Phys. Rev. Lett. **39**, 408 (1977).
[4] D. A. Boyd, F. J. Stauffer, and A. W. Trivelpiece, Phys. Rev. Lett. **37**, 98 (1976).
[5] P. C. Efthimion, V. Arunasalam, and J. C. Hosea, Phys. Rev. Lett. **44**, 396 (1980).
[6] P. C. Efthimion, V. Arunasalam, R. Bitzer, and J. C. Hosea, *Temperature* (Reinhold, New York, 1982), Vol. 5.
[7] N. Bretz, D. Dimock, V. Foote, D. Johnson, D. Long, and E. Tolnas, Appl. Opt. **17**, 192 (1978).
[8] M. A. Goldman and R. A. Bitzer (unpublished).
[9] P. C. Efthimion, V. Arunasalam, R. Bitzer, L. Campbell, and J. C. Hosea, Rev. Sci. Instrum. **50**, 949 (1979).
[10] R. H. Dicke, Rev. Sci. Instrum. **17**, 268 (1946).
[11] K. M. Young *et al.*, Plasma Phys. **26**, 11 (1984).
[12] P. C. Efthimion *et al.*, Phys. Rev. Lett. **52**, 1492 (1984).
[13] R. J. Hawryluk *et al.*, Proceedings of the 3rd International Symposium on Heating in Toroidal Plasmas, Rome, Italy, 1984 (to be published).
[14] K. Hill (private communication).